High-resolution Digital Terrain Model and Land-surface Parameters of São Sebastião and Ilhabela, southeastern Brazil

Rebeca Durço Coelho

Institute of Geosciences, University of São Paulo, São Paulo, 05508-080, Brazil

Gabriella Labate Frugis

Institute of Astronomy, Geophysics and Atmospheric Sciences, University of São Paulo, São Paulo, 05508-090, Brazil

Camila Duelis Viana

Institute of Geosciences, University of São Paulo, São Paulo, 05508-080, Brazil

Carlos H. Grohmann

Institute of Astronomy, Geophysics and Atmospheric Sciences, University of São Paulo, São Paulo, 05508-090, Brazil

Abstract

Effective disaster risk management and detailed environmental studies in landslide-prone regions require high-resolution and accurate Digital Terrain Models (DTMs). This work describes the development of a 2 m-resolution lidar-based DTM and an extensive set of land-surface parameters (LSPs) for the municipalities of São Sebastião and Ilhabela, southeastern Brazil. The dataset was generated from approximately 650 GB of airborne lidar point clouds, processed through a reproducible workflow comprising ground point classification, merging of filtered files, Triangulated Irregular Network (TIN) interpolation, gap filling, and surface smoothing. The resulting high spatial resolution enabled the extraction of topographic parameters for local-scale landslide susceptibility analyses, surpassing the detail of existing photogrammetric and global DEMs for the region, revealing geomorphological features previously indiscernible, including past landslide deposits, drainage captures, and structural lineaments. The resulting products represent the first openly accessible high-resolution DTM for this region, made available via Zenodo, thus supporting applications in landslide susceptibility mapping, environmental modeling, and territorial planning. This open-access initiative contributes to bridging the gap in Brazil's high-resolution topographic data availability and fosters both scientific research and evidence-based decision-making.

Keywords: lidar, geomorphometry, geomorphology, landslide, tectonics, territorial planning

1. Introduction

Digital Elevation Models (DEMs) are ubiquitous datasets in science to represent Earth's surface. More specifically, a Digital Surface Model (DSM) marks the lower boundary of the atmosphere (with the terrain, water bodies, ice, vegetation or human-made objects), while a Digital

Email addresses: rebeca.coelho@usp.br (Rebeca Durço Coelho), gabriella.frugis@usp.br (Gabriella Labate Frugis), camila.viana@usp.br (Camila Duelis Viana), guano@usp.br (Carlos H. Grohmann)

URL: http://orcid.org/0000-0003-2131-8862 (Rebeca Durço Coelho), https://orcid.org/0000-0001-8165-2403 (Gabriella Labate Frugis), http://orcid.org/0000-0001-7093-0244 (Camila Duelis Viana), http://orcid.org/0000-0001-5073-5572 (Carlos H. Grohmann)

Terrain Model (DTM) records the boundary between the terrain (lithosphere) and the atmosphere, without vegetation, buildings etc, also being called a "bare-earth" DEM (Guth *et al.*, 2021).

DEMs can be generated by various means such as InSAR (Interferometric Synthetic Aperture Radar), photogrammetry of optical imagery, and lidar (light detection and ranging), with terrestrial, airborne, or spaceborne sensors (Nelson *et al.*, 2009). Photogrammetry always produces DSMs, since optical images cannot provide information below the canopy (Winsen & Hamilton, 2023). InSAR can produce DSMs or DTMs, depending on the wavelength employed; longer wavelengths may penetrate foliage but shorter wavelengths will be reflected at the top or mid-canopy. Time of data acquisition will also influence the results, due to loss of foliage in temperate forests during autumn (allowing more signal penetration even with shorter wavelengths) or snow coverage in winter (Carabajal & Harding, 2006). Lidar can also produce DSMs or DTMs, as the sensors can register several reflections of the same emitted laser pulse, from the top of canopy, to intermediate objects, through the ground (Fowler *et al.*, 2007).

There are several global (or quasi-global) DEMs available at no cost to the user, such as SRTM (Shuttle Radar Topography Mission – Farr *et al.*, 2007), ASTER GDEM (ASTER Global DEM – Tachikawa *et al.*, 2011), ALOS AW3D30 (ALOS World 3D – Tadono *et al.*, 2015), NASADEM (Crippen *et al.*, 2016), and Copernicus DEM (CopDEM – Strobl, 2020), all distributed at a resolution of 1 arc-second ($\sim 30m$ at the Equator). These are all considered as DSMs due to their methods of generation (InSAR for SRTM and Copernicus DEM, photogrammetry for ALOS AW3D30 and ASTER GDEM), although SRTM and CopDEM show elevations closer to mid-canopy in some regions (Carabajal & Harding, 2006; Guth & Geoffroy, 2021).

Recently, several endeavors have been presented to create DTMs with machine learning methods, based on the global DSMs and ancillary data (local lidar data, land-use maps, etc.). These 'edited DEMs' include FABDEM (Hawker *et al.*, 2022), FathomDEM (Uhe *et al.*, 2025) and GEDTM (Ho *et al.*, 2025) with full global coverage, DeltaDTM (Pronk *et al.*, 2024) and DiluviumDEM (Dusseau *et al.*, 2023), which focus on coastal areas, and ANADEM (Laipelt *et al.*, 2024) covering South America. The DEMIX Initiative (Strobl *et al.*, 2021) carried out extensive comparisons of these DEMs and ranks CopDEM as the best global DSM, noting that SRTM, NASADEM and ASTGER GDEM should be considered legacy datasets (Bielski *et al.*, 2024; Guth *et al.*, 2024).

Country-wide DEMs are commonly based on lidar or photogrammetry of high-resolution orbital or airborne imagery. Examples include the USGS 3D Elevation Program (3DEP), which provides a lidar-based multi-resolution dataset at resolutions of approximately 30, 10 and 3 meters for the conterminous United States and at 1 m for parts of the United States[1]; most European countries offer open access to lidar-based DEMs, as well as New Zealand; Mexico has 1 m and 5 m lidar DEMs for several areas of the country.

Brazil is a country of continental dimensions, but lacks detailed topographic mapping of its territory. Currently, the Federal agency responsible for systematic mapping, IBGE (*Instituto Brasileiro de Geografia e Estatística* – Brazilian Institute for Geography and Statistics), indicates that 100% of the territory is mapped at a 1:250,000 scale, 70% at a 1:100,000, 15% at a 1:50,000, and only 1% at 1:25,000[2].

In the 2010s, a joint initiative of the Brazilian Army and Air Force sought to fill the Amazonian 'cartographic void' (areas with mapping at 1:250,000 or less) with airborne InSAR in a project known as 'Radiography of Amazonia' (RAM) (Grohmann, 2015). The resulting available data are 5 m DSMs distributed under a restrictive license (the data are considered sensitive and cannot be shared with foreign researchers, for example) through the Army's Geoportal[3]. Initially, there was also availability of DTMs and raw radar images, but that data is now of exclusive use of the Brazilian Armed Forces.

In Brazil, each state is responsible for topographic mapping at scales of 1:10,000 or larger.

[1] https://www.usgs.gov/3d-elevation-program - Last access 2025-11-01

[2] Value calculated using the Digital Index Map (4th edition, 2011), based on the 'available' (*disponíveis*) topographic maps (direct download link)

[3] https://bdgex.eb.mil.br/bdgexapp - Last access 2025-11-01

While some states have traditional maps with such level of detail, others are investing in lidar and/or photogrammetric surveys to update their geospatial databases. Photogrammetric DEMs with resolution of 2 m are available for the states of Espírito Santo[4] and Santa Catarina[5], while Bahia[6] and Amapá[7] have partial state coverage of 5 m DEMs from airborne InSAR (the same system used by the RAM project).

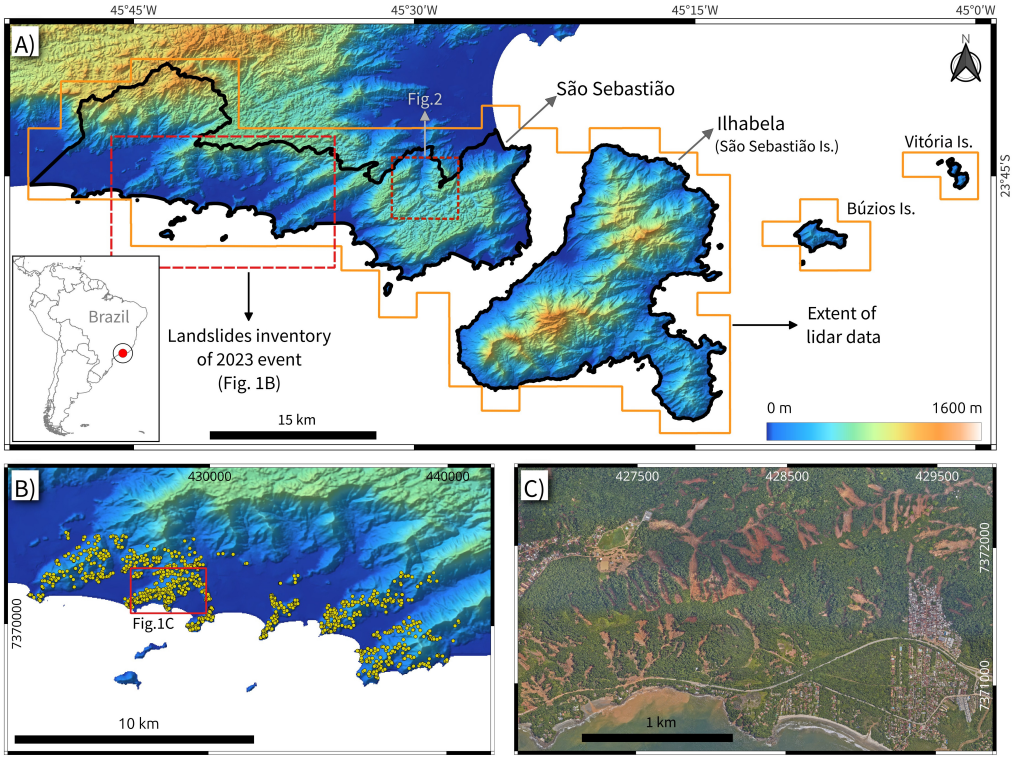

Figure 1: A) Location and morphological context of São Sebastião and Ilhabela municipalities, southeastern Brazil. The thick black line marks the cities' boundaries. Orange line show the limits of lidar data. Terrain morphology from FABDEM (Hawker *et al.*, 2022). Insets (red dashed line), delimits the area of the landslides inventory by Coelho *et al.* (2024) (shown in B) and of Figure 5. B) Landslide inventory for the 2023 event (Coelho *et al.*, 2024). C) Orthophoto of the landslides, surveyed on 2023-02-25 by the São Paulo State Government (IDE-SP, 2023).

São Paulo offers 5 m DSM and DTM for the whole state, although these are interpolated from photogrammetrically-derived point heights with 15 m spacing, and present numerous issues, such as interpolation artifacts and surface texture mismatch between adjacent tiles. Pernambuco was the first state to provide open DSMs and DTMs from lidar surveys[8], with 1 m resolution (Cirilo *et al.*, 2014). Most of the state capitals (and other large cities) have lidar surveys, but do not distribute the data due to a lack of digital infrastructure to host and serve large amounts of data. The city of São Paulo, the most populous city in the country (and fourth in the world, with ~11,450,000 inhabitants), serves two lidar surveys (2017 and 2020) through the city's geoportal, GeoSampa[9]. The data is distributed as point clouds in LAS format. Grohmann & Gomes (2022) created a DSM and a DTM from the 2017 data and hosted them on Kaggle.

The Geographical and Cartographic Institute of São Paulo (IGC-SP – *Instituto Geográfico e Cartográfico do Estado de São Paulo*) the official cartographic agency of the São Paulo State

[4] https://geobases.es.gov.br - Last access 2025-11-01
[5] https://sigsc.sc.gov.br/ - Last access 2025-11-01
[6] Accessible via the Brazilian Army BDGEx Portal
[7] https://sema.portal.ap.gov.br - Last access 2025-11-01
[8] https://pe3d.pe.gov.br/ - Last access 2025-11-01
[9] https://geosampa.prefeitura.sp.gov.br/ - Last access 2025-11-01

coordinate a project to map the entire state area with lidar. The surveys happened between 2023 and 2024. The point clouds have a minimum point density of 10 pts/m^2 in the Metropolitan Region of São Paulo (the city of São Paulo and its neighboring cities) and of 4 pts/m^2 in the rest of the state.

In the night of 18-19th February 2023, a massive rainfall event struck the northern shore of São Paulo State (Fig.1A). In the city of São Sebastião, a precipitation of more than 600 mm in 24h led to widespread landslides, floods and localized debris flows, causing 65 causalities and major infrastructure damage; in the neighboring Ilhabela, the rainfall reached 337 mm and affected mainly its southern region, triggering landslides detectable in aerial imagery on more elevated hillsides (Marengo *et al.*, 2024).

Several inventories of these landslides have been created, using different methods and data. Marengo *et al.* (2024) used PlanetLabs imagery at 3 m resolution to map landslide scars, debris flows, landslide deposits, debris fans, and mud deposits, reporting a total area of almost 2×10^6 m^2. Coelho *et al.* (2024) produced an inventory of the landslides scars (Fig.1B) based on a 10 cm resolution orthomosaic released by the São Paulo State Government only a few days after the disaster (Fig.1C). The inventory contains 1,070 landslide scar polygons and is openly available in Zenodo. Bonini *et al.* (2025) created a landslide inventory for the same area using an object-based Random Forest approach, identifying 396 scars in São Sebastião and 100 in Ilhabela. We do note that both Marengo *et al.* (2024) and Bonini *et al.* (2025) state that their datasets are available upon request, a practice considered inefficient in terms of data sharing by Tedersoo *et al.* (2021).

Table 1: Whitebox tools and parameters for each step of the lidar processing workflow applied to the DTM generation.

Step	**Description**	**WbW Tool**	**Main Parameters**
Step 1	Ground point filtering	`filter_lidar_classes` or `filter_lidar` (WbW Pro)	exclusion_classes = [1, 3–19]
Step 2	Merging filtered LAS files	`lidar_join`	Region-specific files merged
Step 3	TIN interpolation	`lidar_tin_gridding`	cell_size = 2 m, max_triangle_edge = 1,000 m
Step 4	Filling DTM gaps	`fill_missing_data`	filter_size = 51, weight = 2.0, exclude edges
Step 5a	Remove off-terrain objects (Lindsay, 2018)	`remove_off_terrain_objects`	filter_size = 7, slope_threshold = 11.0
Step 5b	Smooth vegetation residual (WbW Pro)	`smooth_vegetation_residual`	max_scale = 15, dev_threshold = 0.06, scale_threshold = 4 (2 passes)
Step 5c	Feature-preserving smoothing (Lindsay *et al.*, 2019a)	`feature_preserving_smoothing`	filter_size = 3, normal_diff_threshold = 12.0, iterations = 1

Efforts to prevent future disasters in the region include improving landslide susceptibility maps for the area. Landslide susceptibility analysis intends to recognize the conditions in which past landslides occurred, and employ that information to determine where new events might happen (Aleotti & Chowdhury, 1999; Guzzetti *et al.*, 2012). A review of such studies in Brazil by Dias *et al.* (2021) revealed that DEMs are widely used to derive land-surface parameters (LSPs – slope, aspect, curvatures, etc) used as input for susceptibility models. Given the scarcity of high-resolution open elevation data in Brazil, researchers resort to global DEMs like SRTM or CopDEM. For example, Varnier (2024) used NASADEM and Random Forest within Google Earth Engine to evaluate landslide susceptibility for the municipalities of São Sebastião and Ilhabela, mapping 5.4% of the area as highly susceptible. Alcântara *et al.* (2024) used a weighted sum model to develop susceptibility maps for four climate scenarios from the Intergovernmental Panel on Climate Change (IPCC), but did not specify the source of the elevation data.

While the resolution of ∼30 m might be enough for regional-scale analysis, it lacks the angular coherence between neighboring pixels necessary to derive LSPs for detailed studies (Hengl, 2006;

Valeriano *et al.*, 2006; Grohmann *et al.*, 2007). Moreover, each pixel represents an area of ∼900 m^2, which can be larger than entire small landslides.

To properly study landslide susceptibility on a local scale, lidar data are the best option. If data is acquired before a landslide event, DTMs with 1–5 m resolution can faithfully represent the topography and derived LSPs. In the case of post-event surveys, one can calculate the difference between the DSM and the DTM, to highlight the scars and deposit areas.

After negotiations with the IGC-SP, our research group obtained access to the raw lidar data for São Sebastião and Ilhabela, in order to produce landslide susceptibility maps based on a high-resolution DTM, and to provide technical feedback to IGC-SP on the quality of the data. Although raw data cannot be shared, derivative products, such as DEMs and LSPs, can. Therefore, following the principles of Open Science (OECD, 2015), in this paper we describe a high-resolution dataset of elevation and land-surface parameters derived from the lidar data. We understand these data are invaluable not only to academic researchers studying the region, but also to policymakers and the Public Administration.

2. Data and Methods

The data used in this study consist of raw airborne lidar point cloud files in LAS format, totaling approximately 650 GB of data. The data cover the entire area of the municipalities of São Sebastião and Ilhabela (Fig. 1).

The LAS files follow the ASPRS LAS 1.4 specification (ASPRS, 2011) and include standard point attributes such as XYZ coordinates, intensity, return number, number of returns, classification, and GPS time. All data are provided in the WGS84 / UTM zone 23S coordinate reference system (EPSG:32723), with altimetric information converted to Normal (H^N) using the `hgeoHNOR2020` model provided by IBGE (IBGE, 2023). Point classification encompasses ground, low/medium/high vegetation, and buildings. The ground point density varies across acquisition blocks, with an average of 0.32 points per square meter, ensuring sufficient detail to generate digital terrain models with a grid spacing of 2 m (Anderson *et al.*, 2006; Hengl, 2006).

All data processing and analysis steps were performed using a combination of open-source and proprietary tools. Specifically, we employed WhiteboxTools[10] (WbT) and Whitebox Workflows[11] (WbW) libraries (Lindsay, 2016) for lidar data processing and terrain analysis. The task 'smooth vegetation residual' was performed using Whitebox Workflows Professional, the commercial version of the Whitebox suite, which offers extended functionality for point cloud manipulation and surface modeling.

2.1. Lidar Data Processing and DTM Generation

The lidar data processing workflow consisted of five main stages: ground point filtering, merging of filtered files, DTM generation via TIN interpolation, gap filling in the DTM, and subsequent surface smoothing (Table 1). All raster outputs at each stage were exported in compressed TIFF format to optimize storage and ensure compatibility with subsequent analyses. Throughout the workflow, file/object existence checks and systematic memory management were applied to enhance computational efficiency and guarantee reproducibility.

When examining the point cloud classification for the small islands and the shoreline of the main island of the Ilhabela Archipelago, discrepancies were found between the assigned classes and the actual surface conditions (Fig. 2). In several rocky areas with no vegetation cover, no ground-classified points were present. A similar issue occurred in the interior of the smaller islands, despite their vegetation density being comparable to that of the main island, where the classification appeared correct.

[10] https://www.whiteboxgeo.com/manual/wbt_book/intro.html
[11] https://www.whiteboxgeo.com/manual/wbw-user-manual/book/preface.html

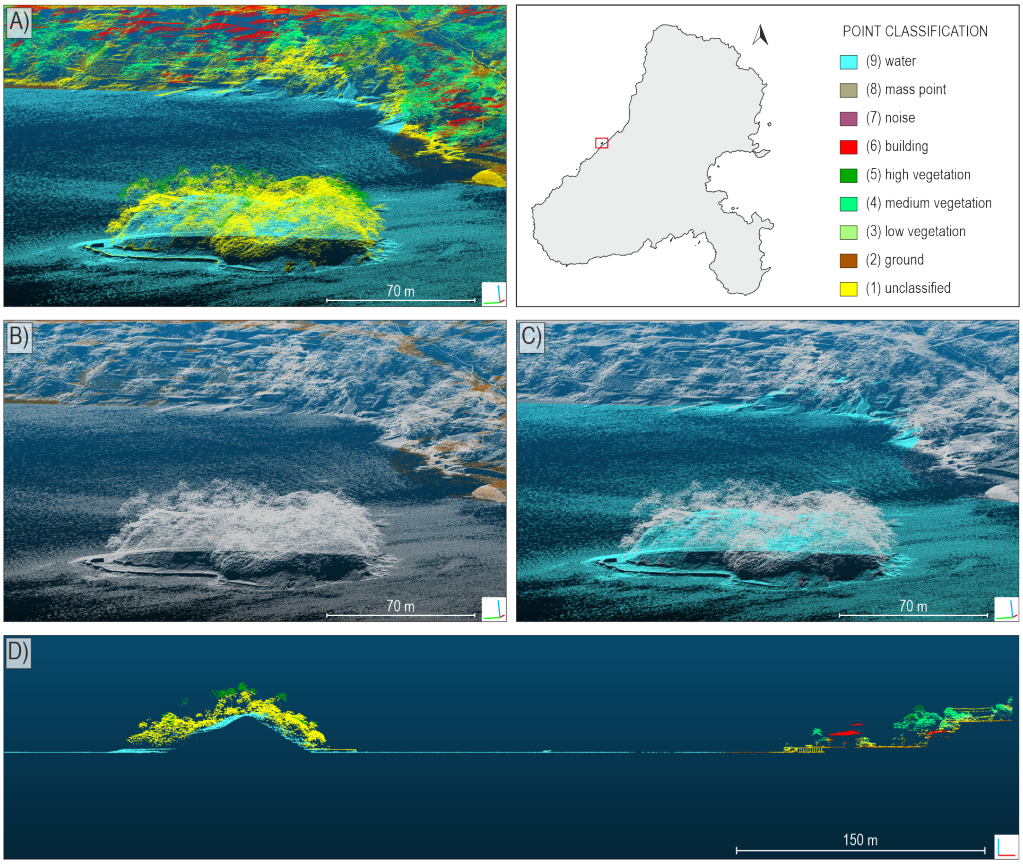

Figure 2: Perspective view of the Ilha das Cabras point cloud (Ilhabela), showing the misclassification along land-water boundaries. A) All classes. B) Ground-classified points in orange-brown. C) Water-classified points in cyan. D) Cross-section view showing water-classified points extending over the land area of Ilha das Cabras.

In these problematic regions, a large number of points had been classified as water, even though they clearly corresponded to land. An inspection in CloudCompare (Girardeau-Montaut, 2019) confirmed that these water-classified points were in fact ground points. The most likely cause is that, in areas close to the sea, the classification algorithm failed to correctly distinguish the land–water boundary.

To address this issue, we delineated the coastlines of the smaller islands and applied a shoreline buffer around the main island. The original point cloud files were then clipped to these polygons, and the `filter_lidar` tool (WbW Pro) was applied to retain the last and single returns of water-classified points, thereby correcting the classification error in these coastal areas. Using the `lidar_join` tool, these filtered points were merged with the ground-classified points previously filtered.

2.2. DTM altimetric assessment

The study area's rugged topography, characterized by steep escarpments and dense Atlantic Forest cover, imposes severe logistical constraints on geodetic infrastructure. Consequently, the regional geodetic network is sparse, comprising only five active stations (Figure 3), which were not used in the altimetric assessment. Data and metadata for the IBGE stations can be accessed through the Brazilian Geodetic Database (BDG–IBGE)[12]. As an alternative, elevation control points were extracted from 1:10,000 scale topographic maps produced by IGC-SP. Even though

[12] http://www.bdg.ibge.gov.br/appbdg/

these maps were produced in the 1970s, they are the most detailed topographic information published for the study area.

Figure 3: DTM extent and spatial distribution of elevation reference points and IBGE geodetic stations. White crosses represent the IGC topographic spot heights (1:10,000 scale) used for DTM assessment. Triangles indicate IBGE geodetic stations. Background: Esri "World Imagery".

This reliance on historical mapping introduces a significant methodological challenge: the 1970s cartography, while compliant with its era's standards, lacks the vertical precision of modern active sensors. Therefore, this analysis is framed not as an absolute validation, but as a *cross-comparison assessment* to quantify the consistency between the lidar-derived DTM and the available cartographic records.

These maps are currently distributed through the São Paulo State Spatial Data Infrastructure (IDE-SP)[13] and were accessed via Web Map Service (WMS) protocol in QGIS.

After loading the topographic maps via WMS, 30 spot height points were selected within the spatial extent of each DTM – approximately 524 km^2 for São Sebastião and 347 km^2 for Ilhabela (Figure 3, and Supplementary Material). Priority was given to locations on forested hilltops and stable natural slopes, to ensure spatial representativeness while accounting for the region's predominant land cover (>80%). This sampling size follows the base recommendations for project areas $\leq$ 1000 km^2 according to Table C.1 of the ASPRS 2024 standards (ASPRS, 2024).

Given the extreme accessibility constraints, these 30 points serve as a hybrid sample to characterize discrepancies in both non-vegetated and vegetated environments, traditionally referred to as Non-vegetated (NVA) and Vegetated Vertical Accuracy (VVA). Furthermore, the results must be interpreted within the context of the $\sim$ 50 year gap between the original photogrammetric restitution and the lidar acquisition. Geomorphological processes, erosion, and land-use changes during this interval, coupled with the inherent limitations of airborne photogrammetry in dense canopy, contribute to the observed residuals.

The vertical discrepancy, hereafter referred to as the *Vertical Residual* (R_v), was calculated by subtracting the 1978 topographic elevation from the lidar-derived elevation:

$$R_v = Elevation_{lidar} - Elevation_{IGC} \quad (1)$$

[13] https://www.idesp.sp.gov.br/geonetwork/srv/por/catalog.search#/metadata/b295f3cb-9e03-44e6-80db-f929b252418f

Where $Elevation_{lidar}$ represents the orthometric height from the 2-m lidar-derived DTM and $Elevation_{IGC}$ corresponds to the spot heights extracted from the IGC topographic maps.

The vertical consistency of each model was subsequently quantified using the Root Mean Square Error (RMSE – eq. 2), Mean Error (Bias – eq. 3), and the Standard Deviation (σ – eq. 4) of the residuals:

$$RMSE = \sqrt{\frac{1}{n}\sum_{i=1}^{n} R_{v,i}^2} \tag{2}$$

$$Bias = \bar{R}_v = \frac{1}{n}\sum_{i=1}^{n} R_{v,i} \tag{3}$$

$$\sigma = \sqrt{\frac{1}{n}\sum_{i=1}^{n}(R_{v,i} - \bar{R}_v)^2} \tag{4}$$

Where n is the number of reference points, and $R_{v,i}$ is the vertical residual for each point.

It is essential to emphasize that R_v is a composite metric. It incorporates the propagated uncertainty from three primary sources: (i) the intrinsic precision of the lidar-derived DTM; (ii) the nominal accuracy of the 1:10,000 scale topographic maps; and (iii) the environmental changes occurred since the 1970s. Conceptually, this residual does not represent an absolute measurement of sensor error, but rather a *methodological discrepancy.*

Statistical results (Table 2) show RMSE values of 2.55 m for São Sebastião and 2.44 m for Ilhabela, classifying the models within the 300-cm Vertical Accuracy Class according to ASPRS (2024) standards. The consistent negative bias (−1.61 m and −1.89 m) indicates that the lidar elevations are lower than those found in the 1:10,000 topographic reference. This trend is attributed to the lidar's capability to penetrate the forest canopy and reach the terrain surface, whereas the 1978 photogrammetric mapping likely registered an intermediate position between the ground and the top of canopy in these densely forested areas.

Table 2: Vertical Accuracy Metrics for DTM Assessment

	Dependent variable: Vertical Residual (R_v)				
Area	Bias (m)	RMSE (m)	SD (σ) (m)	Min (m)	Max (m)
São Sebastião	−1.61	2.55	2.02	−4.87	0.83
Ilhabela	−1.89	2.44	1.57	−4.89	1.61
Check points (n)	60 (30 per area)				
Reference Scale	1:10,000 (IGC Topographic Maps)				
Vertical Datum	Imbituba (SGB)				

In these steep and forested areas, the 1978 photogrammetric restitution was limited by the inability of passive sensors to penetrate dense foliage. The negative residuals observed here represent the successful removal of this "vegetation noise" by the lidar pulses. Thus, the observed discrepancies are primarily attributed to the transition from manual, vegetation-influenced restitution to high-resolution active remote sensing, rather than intrinsic sensor failure.

This interpretation is visually confirmed by the distribution of residuals (Figure 4). The histograms and boxplots reveal that the error mass is consistently shifted below the zero-baseline, while the scatter plot shows the 2m-DTM elevations following the 1:1 identity line with a constant downward offset. As per ASPRS (2024) guidelines, diagnosing such systematic offsets is critical for data transparency and for the legitimate use of pre-existing cartography as a baseline for modern geoscientific modeling.

2.3. Land-surface parameters and objects

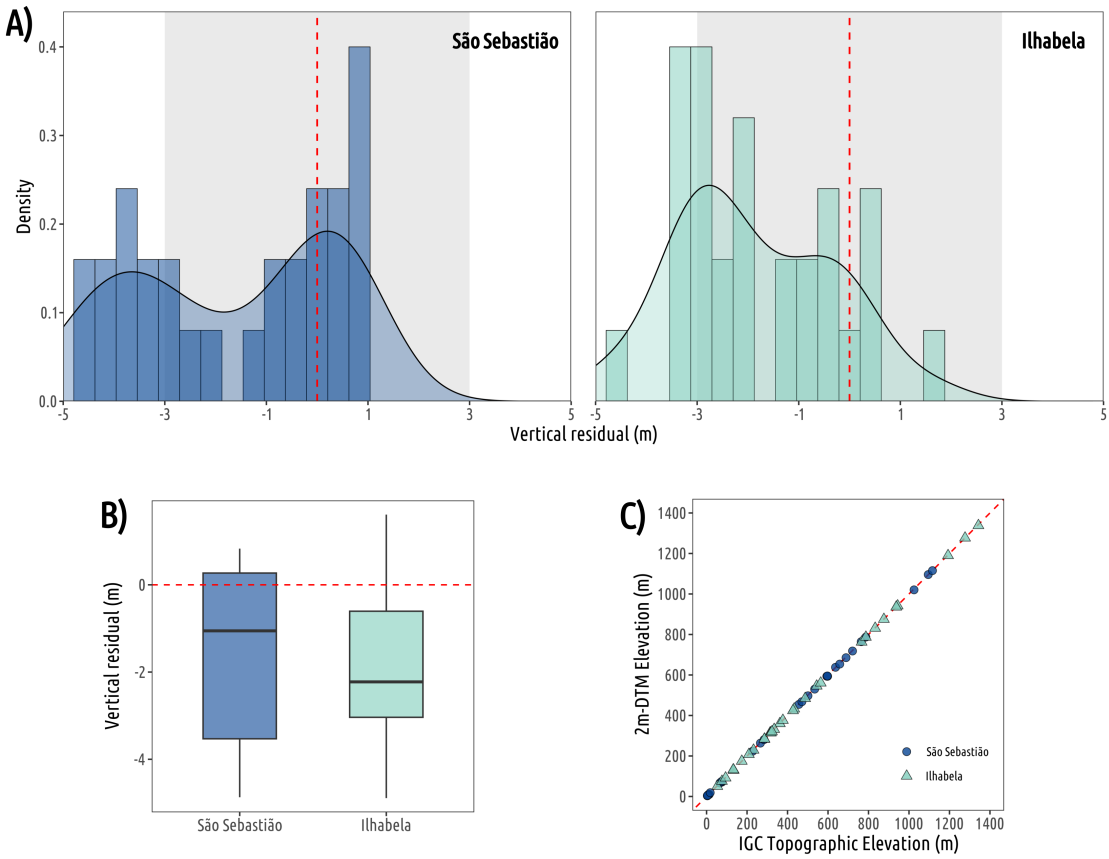

Figure 4: Vertical accuracy assessment of the 2m-DTM. (A) Density distribution of residuals (R_v); (B) Boxplot showing the dispersion of vertical residuals; (C) Correlation between $Elevation_{IGC}$ and $Elevation_{lidar}$.

Land-surface parameters (LSPs) and land-surface objects (LSOs) are the two DEM-derived entities fundamental to modern geomorphometry (Mark & Smith, 2004; Pike *et al.*, 2009). An LSP is a descriptive and quantitative measure of surface characteristics, such as slope, aspect, and curvatures. An LSO is a discrete spatial feature, such as a drainage network, ridge, or watershed lines. We provide a set of 17 LSPs and LSOs, that comprise several facets of the landscape, including illumination, shape, landform characteristics, and hydrology.

Figure 5 shows an example of three LSPs (hillshade, slope and surface roughness) for the 2 m lidar DTM (Fig. 5 A/B/C), a 5 m photogrammetric DTM from IDE-SP (Fig. 5 D/E/F), and the 30 m FABDEM DTM (Fig. 5 G/H/I). The area is almost completely covered by dense forests, and was selected to illustrate not only the effectiveness of our processing workflow, providing a clean surface while preserving the sharpness of ridgelines, but also some issues with the other datasets. The 5 m DTM has a clear north-south division in two areas with contrasting texture, indicating poor vegetation filtering. FABDEM shows an issue often overlooked by DEM users, linear artifacts caused by cell size adjustment due to projection from Lat-Long to UTM (Grohmann & Steiner, 2008).

Hillshade, or shaded relief, is a technique of terrain visualization considering the orientation of a light source and the local slope and aspect (Horn, 1981; Imhof, 1982). We used the tool `multidirectional_hillshade`, and set altitude to 30 °, and Z-factor to 1 as default.

Slope steepness was calculated with the `slope` tool, with the output in degrees. Since the data are in a projected coordinate system, this tool uses a polynomial fit of the elevations within the 5x5 neighborhood surrounding each cell (Florinsky, 2016).

Aspect, the slope orientation in degrees clockwise from north, was calculated with the `aspect`

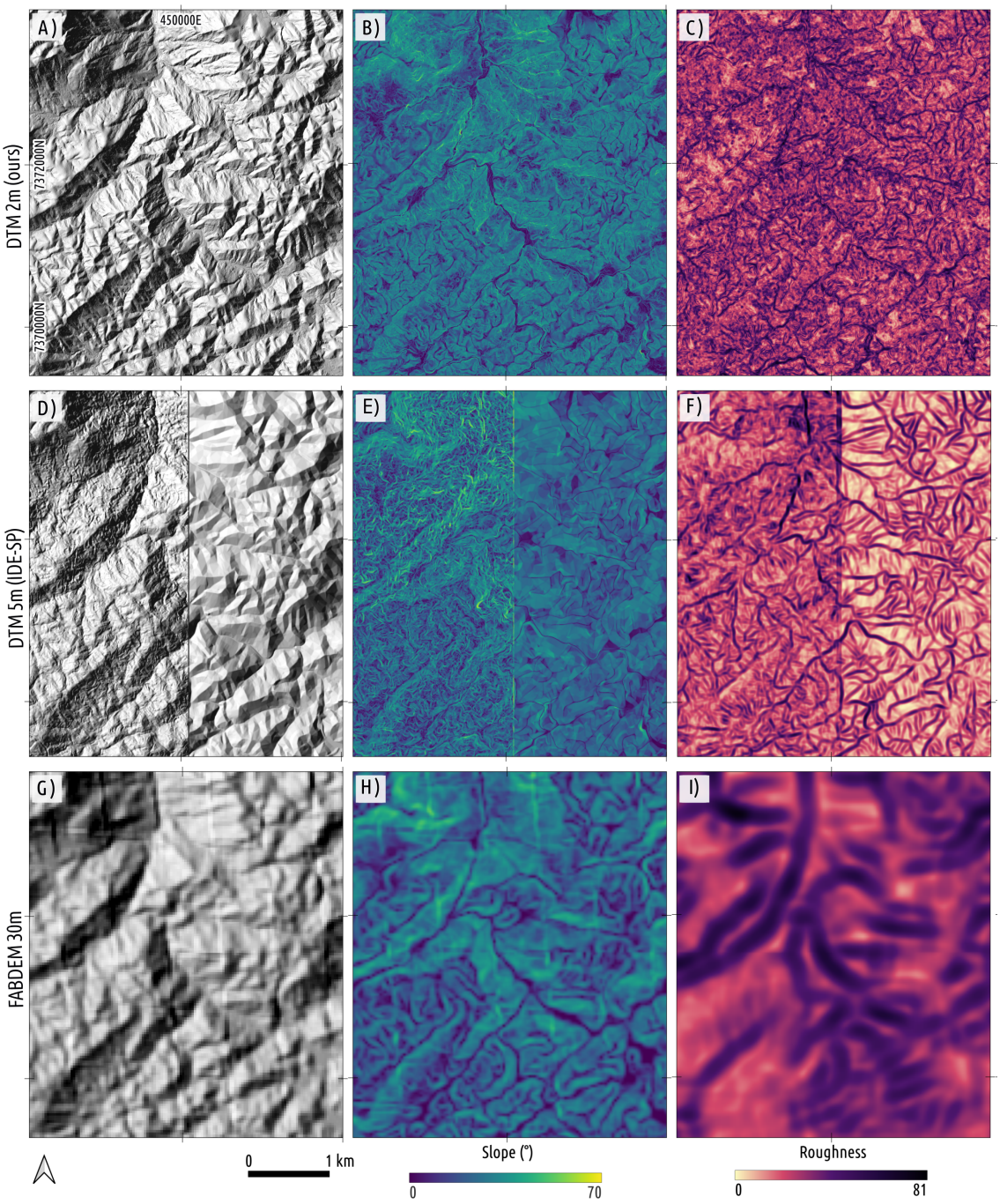

Figure 5: Comparison of terrain parameters derived from high-resolution (DTM 2 m), intermediate resolution (DTM 5 m from IDE-SP), and coarse resolution (FABDEM 30 m) DEMs for the study area. Location of area shown in Fig. 1. A/D/G: Hillshade. B/E/H: Slope. C/F/I: Surface roughness.

tool, using a 5x5 neighborhood of each cell (Florinsky, 2016).

Profile Curvature is the rate of change in slope along a flow line, and characterizes the degree of downslope acceleration or deceleration (Gallant & Wilson, 2000). Profile curvature is negative for slope increasing downhill (convex) and positive for slope decreasing downhill (concave). We used the tool `profile_curvature`, with output in units of m^{-1}.

Plan Curvature (or contour curvature), is the rate of change in aspect along a contour line,

and characterizes the degree of flow convergence or divergence within the landscape (Gallant & Wilson, 2000). Plan curvature is negative for diverging flow and positive for convergent areas. We used the tool `plan_curvature`, with output in units of m^{-1}.

Minimal Curvature is the curvature of a principal section with the lowest value of curvature at a given point of the topography (Florinsky, 2017). Positive values correspond to hills while negative values correspond to valley positions (Florinsky, 2016). We used the tool `minimal_curvature`, with output in units of m$^-$1, and set the `log_transform` option to `True`.

Maximal Curvature is the curvature of a principal section with the highest value of curvature at a given point of the topography (Florinsky, 2017). Positive values correspond to ridges while negative values indicate closed depressions (Florinsky, 2016). We used the tool `maximal_curvature`, with output in units of m$^-$1, and set the `log_transform` option to `True`.

Difference from Mean Elevation is the difference between the elevation of each grid cell and the mean elevation of its local neighborhood, being a measurement of relative topographic position. We used the tool `difference_from_mean_elevation`, and set `filterx` and `filterx` to 11 grid cells.

Shape Index (Koenderink & van Doorn, 1992) is a dimensionless variable ranging from -1 to 1, useful for landform classification. Positive values indicate convex landforms, and negative values correspond to concave landforms (Florinsky, 2017). Absolute values from 0.0 to 0.5 are characteristic of hyperbolic forms (saddles), while absolute values from 0.5 to 1.0 are associated with elliptic forms (hills and closed depressions). We used the tool `shape_index`, which requires a license for Whitebox Workflows for Python Professional.

The **Geomorphons** landform classification is based on a line-of-sight analysis for the eight topographic profiles in the cardinal directions surrounding each grid cell of the input DEM (Jasiewicz & Stepinski, 2013). We used the `geomorphons` tool with default parameters.

Spherical Standard Deviation of Normals measures the angular dispersion of the surface normal vectors within a local neighborhood, being a measure of *surface roughness*, complexity, and texture (Grohmann *et al.*, 2011; Lindsay *et al.*, 2019b). We used the tool `spherical_std_dev_of_normals`, and set `filter_size` to 11 grid cells.

Flow Accumulation was calculated with the multiple-flow-direction (MFD) algorithm from (Qin *et al.*, 2007). The DTM was pre-processed with the `breach_depressions_least_cost` tool (Lindsay & Dhun, 2015) with the `max_dist` set to 900 m. We then used the `qin_flow_accumulation` tool, with `out_type` set to `sca` (specific contributing area – the catchment area divided by the flow width), and `log_transform` set to `False`.

Wetness Index describes the tendency for a site to be saturated to the surface, given its contributing area and local slope characteristics. This raster was calculated with the `wetness_index` tool, using the flow accumulation and slope rasters as inputs.

Flow Direction is commonly used as input for other spatial hydrology and stream network analysis. In the Whitebox suite, this is calculated with the `d8_pointer` tool, which is based on the D8 algorithm (O'Callaghan & Mark, 1984).

A **Stream network** can be derived from a DEM based on a flow accumulation raster and a specified threshold, which represents the minimum area required to initiate and maintain a channel. We used the `extract_streams` tool with the flow accumulation raster as input and the `threshold` set to 4000 for São Sebastião and 1500 for Ilhabela.

3. Topographic features of interest

Upon inspection of the DTM and derived LSPs, several interesting topographic features were identified, including evidence of past large landslide deposits, river captures and subvolcanic landforms. A selection of examples is shown in Figure 6.

Past landslides indications are highlighted in profile curvature maps by convex and concave landform patterns. Figure 6A shows colluvial deposits from past landslides just north of Vila Sahy, an area heavily affect by the event of 2023. A relic landslide scarp is visible in Fig. 6D, to the west of Castelhanos Beach in Ilhabela.

A drainage capture is shown in Fig. 6B, where a small drainage bends abruptly (indicated by a white arrow) before flowing south from the plateau. Over the plateau a trellis drainage pattern is observed, indicating a structural control over the stream network. Large tectonic lineaments are seen in Fig. 6C: an E-W lineament is marked by black arrows, and a curvilinear structure is indicated by white arrows.

In Fig. 6E, the slope map highlights concentric circular ridges of the Serraria Stock, which is part of the 88-85 Ma alkaline plutonic event of the Serra do Mar Province (Sato, 2006; Sato *et al.*, 2008; Giraldo-Arroyave *et al.*, 2021). In Fig. 6F, a flat-bottomed depression is visible in a surface roughness map, just north of Indaiaúba Beach; this depression is not clearly identifiable in optical imagery due to dense forest cover.

4. Conclusions

This study presents the first publicly available high-resolution Digital Terrain Model (i.e., 'bare-earth') and a comprehensive set of land-surface parameters (LSPs) for the municipalities of São Sebastião and Ilhabela, southeastern Brazil, derived from airborne lidar data. The 2 m-resolution DTM significantly enhances the representation of topographic features when compared to existing regional and global elevation datasets, allowing the identification of subtle geomorphological structures relevant to landslide susceptibility assessment and environmental studies. By providing an open-access dataset processed with a transparent and reproducible workflow, this work contributes to filling a critical gap in Brazil's high-resolution topographic data availability, promoting applications that range from scientific research to disaster risk management and territorial planning. Future work should explore the integration of this dataset with multitemporal remote sensing products and climate projections to refine hazard models and support adaptive strategies in vulnerable mountainous regions.

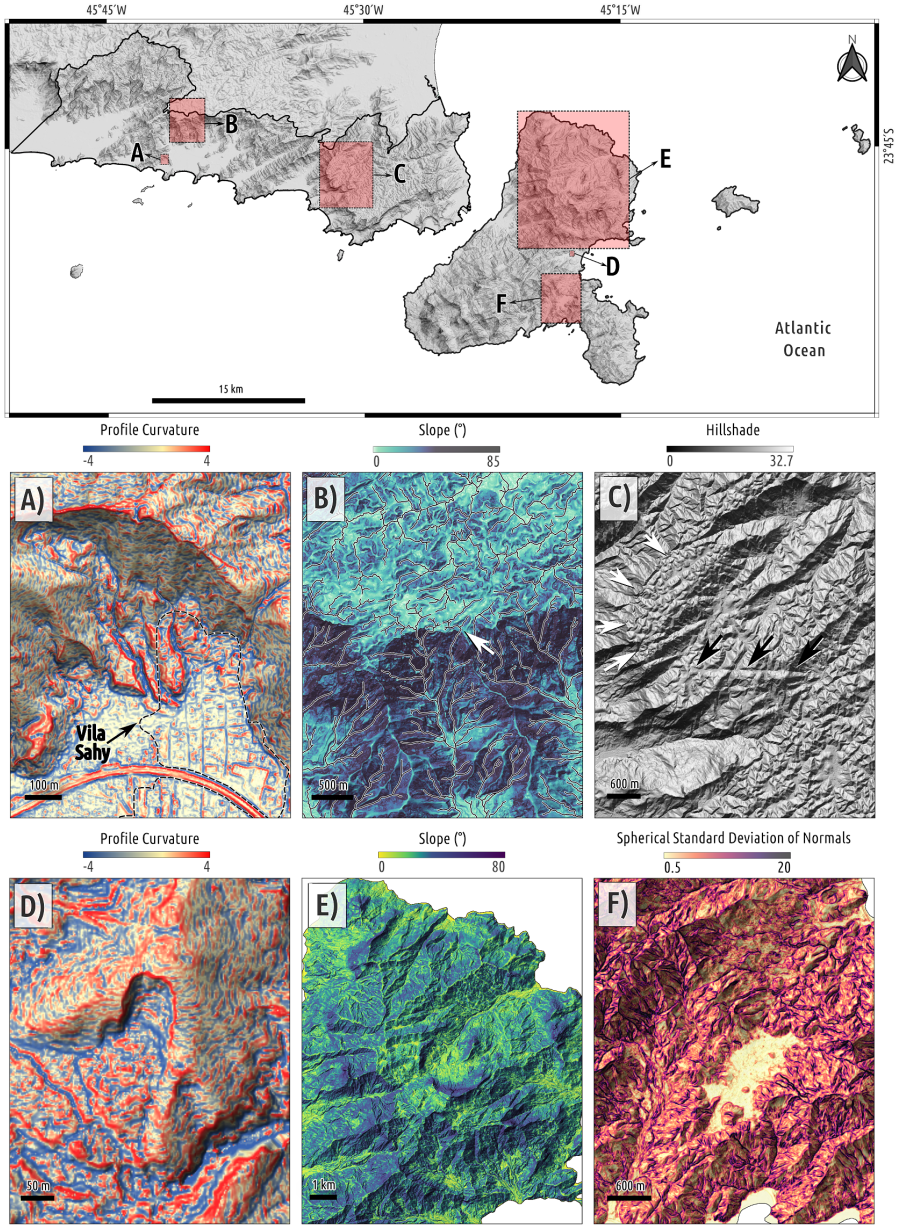

Figure 6: Examples of relevant topographic features identified within the study area, based on different terrain variables derived from the Digital Terrain Model (DTM). A) Deposits of past landslides in the Vila Sahy region, highlighted by convex and concave landform patterns; B) Drainage capture at the transition between the plateau and the escarpment (indicated by the white arrow); C) Structural lineaments revealed by variations in terrain illumination (black and white arrows); D) Scarp of a past landslide with a prominent colluvial deposit downslope; E) Concentric circular ridges, associated with subvolcanic alkaline plutonism; F) Flat-bottom depression evidenced by low surface roughness compared to the surrounding area.

5. Dataset Reference

Coelho, R.D., Frugis, G.L., Viana, C.D., Grohmann, C.H., 2025. High-resolution Digital Terrain Model and Land-surface Parameters of São Sebastião, southeastern Brazil. *Zenodo*. DOI: http://dx.doi.org/10.5281/zenodo.16903678

Frugis, G.L., Coelho, R.D., Viana, C.D., Grohmann, C.H., 2025. High-resolution Digital Terrain Model and Land-surface Parameters of Ilhabela, southeastern Brazil. *Zenodo*. DOI: http://dx.doi.org/10.5281/zenodo.16903853

Acknowledgments

This project was supported by The São Paulo Research Foundation (FAPESP – grant #2023/11197-1) and CNPq (grant #311209/2021-1). R.D.C. is a PhD students finance by the Brazilian Federal Agency for Support and Evaluation of Graduate Education (CAPES – Finance Code 001). G.L.F. is a post-doc researcher financed by CAPES PIPD (grant 88887.122984/2025-00). We are thankful to John B. Lindsay (Guelph University) for providing a license of Whitebox Tools Pro and for assistance in lidar data processing. Raw lidar data was kindly provided by the Geographical and Cartographic Institute of São Paulo, under a data transfer agreement with C.H.G: *Base cartográfica: Nuvem de Pontos LiDAR 2023/2024, 4 a 10 pontos/m^2, pertencentes ao Instituto Geográfico e Cartográfico – IGC, Sistema Cartográfico do Estado de São Paulo.* Acknowledgments are extended to the Editor-in-Chief and the anonymous reviewers for their criticism and suggestions, which helped to improve this paper.

Data Availability Statement

The data that support the findings of this study are available in Zenodo at http://dx.doi.org/10.5281/zenodo.16903678 and http://dx.doi.org/10.5281/zenodo.16903853

References

Alcântara, E., Baião, C.F., Guimarães, Y.C., Mantovani, J.R., Marengo, J.A., 2024. Machine learning approaches for mapping and predicting landslide-prone areas in São Sebastião (Southeast Brazil). *Natural Hazards Research*. http://dx.doi.org/10.1016/j.nhres.2024.10.003

Aleotti, P., Chowdhury, R., 1999. Landslide hazard assessment: summary review and new perspectives. *Bulletin of Engineering Geology and the Environment*, 58(1):21–44. http://dx.doi.org/10.1007/s100640050066

Anderson, E.S., Thompson, J.A., Crouse, D.A., Austin, R.E., 2006. Horizontal resolution and data density effects on remotely sensed LIDAR-based DEM. *Geoderma*, 132(3–4):406–415. http://dx.doi.org/10.1016/j.geoderma.2005.06.004

ASPRS, 2011. *LAS Specification Version 1.4 – R14*. American Society for Photogrammetry and Remote Sensing, Bethesda, MD. Accessed: 2025-07-07. https://www.asprs.org/wp-content/uploads/2019/03/LAS_1_4_r14.pdf

ASPRS, 2024. *American Society for Photogrammetry and Remote Sensing (ASPRS) Positional Accuracy Standards for Digital Geospatial Data*, edition 2 edition. http://dx.doi.org/10.14358/ASPRS.PAS.2024

Bielski, C., López-Vázquez, C., Grohmann, C.H., Guth, P.L., Hawker, L., Gesch, D., Trevisani, S., Herrera-Cruz, V., Riazanoff, S., Corseaux, A., Reuter, H.I., Strobl, P., 2024. Novel approach for ranking DEMs: Copernicus DEM improves one arc second open global topography. *IEEE Transactions on Geoscience & Remote Sensing*, 62:1–22. http://dx.doi.org/10.1109/TGRS.2024.3368015

Bonini, J.E., Martins, T.D., Sugiyama, M.T.d.O., Vieira, B.C., 2025. Landslide inventory of the 2023 serra do mar disaster (brazil). *Discover Geoscience*, 3(1):40. http://dx.doi.org/10.1007/s44288-025-00153-2

Carabajal, C.C., Harding, D.J., 2006. SRTM C-band and ICESat laser altimetry elevation comparisons as a function of tree cover and relief. *Photogrammetric Engineering & Remote Sensing*, 72(3):287–298. http://dx.doi.org/10.14358/PERS.72.3.287

Cirilo, J.A., Alves, F.H.B., Silva, L.A.C., Campos, J.H.A.L., 2014. Suporte de informações georreferenciadas de alta resolução para implantação de infraestrutura e planejamento territorial. *Revista Brasileira de Geografia Física*, 7(4):755–763.
http://dx.doi.org/10.26848/rbgf.v7.4.p755-763

Coelho, R.D., Viana, C.D., Dias, V.C., Grohmann, C.H., 2024. Landslides of the 2023 summer event of São Sebastião, southeastern Brazil: spatial dataset. *Brazilian Journal of Geology*, 54:e20240006.
http://dx.doi.org/10.1590/2317-4889202420240006

Crippen, R., Buckley, S., Agram, P., Belz, E., Gurrola, E., Hensley, S., Kobrick, M., Lavalle, M., Martin, J., Neumann, M., Nguyen, Q., Rosen, P., Shimada, J., Simard, M., Tung, W., 2016. Nasadem global elevation model: Methods and progress. *The International Archives of the Photogrammetry, Remote Sensing and Spatial Information Sciences*, XLI-B4:125–128.
http://dx.doi.org/10.5194/isprs-archives-XLI-B4-125-2016

Dias, H.C., Hölbling, D., Grohmann, C.H., 2021. Landslide Susceptibility Mapping in Brazil: A Review. *Geosciences*, 11(10):425.
http://dx.doi.org/10.3390/geosciences11100425

Dusseau, D., Zobel, Z., Schwalm, C.R., 2023. Diluviumdem: Enhanced accuracy in global coastal digital elevation models. *Remote Sensing of Environment*, 298:113812.
http://dx.doi.org/10.1016/j.rse.2023.113812

Farr, T.G., Rosen, P.A., Caro, E., Crippen, R., Duren, R., Hensley, S., Kobrick, M., Paller, M., Rodriguez, E., Roth, L., Seal, D., Shaffer, S., Shimada, J., Umland, J., Werner, M., *et al.*, 2007. The Shuttle Radar Topography Mission. *Review of Geophysics*, 45:RG2004.
http://dx.doi.org/10.1029/2005RG000183

Florinsky, I.V., 2016. *Digital Terrain Analysis in Soil Science and Geology*. Elsevier.

Florinsky, I.V., 2017. An illustrated introduction to general geomorphometry. *Progress in Physical Geography: Earth and Environment*, 41(6):723–752.
http://dx.doi.org/10.1177/0309133317733667

Fowler, R., Samberg, A., Flood, M.J., Greaves, T.J., 2007. *Digital Elevation Model Technologies and Applications: The DEM Users Manual*, chapter Topographic and terrestrial lidar, pages 119–252. Amer. Soc. Photogramm. Remote Sens, Bethesda, MD, 2nd edition.

Gallant, J.C., Wilson, J.P., 2000. Primary topographic attributes. In J.P. Wilson, J.C. Gallant, editors, *Terrain Analysis: Principles and Applications*, pages 51–86. John Wiley, Hoboken, N.J.

Giraldo-Arroyave, M.I., Vlach, S.R.F., Vasconcelos, P.M., 2021. New high-precision 40 ar/39 ar ages for the serra do mar alkaline magmatism in the são sebastião island, se brazil, and implications. *Brazilian Journal of Geology*, 51:e20210046.
http://dx.doi.org/10.1590/2317-4889202120210046

Girardeau-Montaut, D., 2019. Cloudcompare (version 2.10.3 zephyrus).
http://www.cloudcompare.org/

Grohmann, C.H., 2015. Radiography of the Amazon DSM/DTM data: comparative analysis with SRTM, ASTER GDEM. In *Geomorphometry 2015*.
http://www.geomorphometry.org/Grohmann2015 Poznam, Poland.

Grohmann, C.H., Gomes, F., 2022. Digital Terrain and Surface Models of São Paulo.
http://dx.doi.org/10.34740/KAGGLE/DS/1915612

Grohmann, C.H., Riccomini, C., Alves, F.M., 2007. SRTM-based morphotectonic analysis of the Poços de Caldas Alkaline Massif, southeastern Brazil. *Computers & Geosciences*, 33:10–19.
http://dx.doi.org/10.1016/j.cageo.2006.05.002

Grohmann, C.H., Smith, M.J., Riccomini, C., 2011. Multiscale Analysis of Topographic Surface Roughness in the Midland Valley, Scotland. *Geoscience and Remote Sensing, IEEE Transactions on*, 49(4):1200–1213.
http://dx.doi.org/10.1109/TGRS.2010.2053546

Grohmann, C.H., Steiner, S.S., 2008. SRTM resample with Short Distance-Low Nugget Kriging. *International Journal of Geographical Information Science*, 22(8):895–906.
http://dx.doi.org/10.1080/13658810701730152

Guth, P.L., Geoffroy, T.M., 2021. LiDAR point cloud and ICESat-2 evaluation of 1 second global digital elevation models: Copernicus wins. *Transactions in GIS*, n/a(n/a).
http://dx.doi.org/10.1111/tgis.12825

Guth, P.L., Trevisani, S., Grohmann, C.H., Lindsay, J.B., Gesch, D., Hawker, L., Bielski, C., 2024. Ranking of 10 Global One-Arc-Second DEMs Reveals Limitations in Terrain Morphology Representation. *Remote Sensing*, 16(17).
http://dx.doi.org/10.3390/rs16173273

Guth, P.L., Van Niekerk, A., Grohmann, C.H., Muller, J., Hawker, L., Florinsky, I.V., Gesch, D., Reuter, H.I., Herrera-Cruz, V., Riazanoff, S., López-Vázquez, C., Carabajal, C.C., Albinet, C., Strobl, P., 2021. Digital Elevation Models: Terminology and Definitions. *Remote Sensing.*, 13(18):3581.
http://dx.doi.org/10.3390/rs13183581

Guzzetti, F., Mondini, A.C., Cardinali, M., Fiorucci, F., Santangelo, M., Chang, K.T., 2012. Landslide inventory maps: New tools for an old problem. *Earth-Science Reviews*, 112(1–2):42–66.
http://dx.doi.org/10.1016/j.earscirev.2012.02.001

Hawker, L., Uhe, P., Paulo, L., Sosa, J., Savage, J., Sampson, C., Neal, J., 2022. A 30 m global map of elevation with forests and buildings removed. *Environmental Research Letters*, 17(2):024016.

http://dx.doi.org/10.1088/1748-9326/ac4d4f
Hengl, T., 2006. Finding the right pixel size. *Computers and Geosciences*, 32(9):1283–1298.
http://dx.doi.org/10.1016/j.cageo.2005.11.008
Ho, Y.F., Grohmann, C. H. Lindsay, J., Reuter, H.I., Parente, L., Witjes, M., Hengl, T., 2025. GEDTM30: Global Ensemble Digital Terrain Model at 30 m and Derived Multiscale Terrain Variables. *PeerJ*, 13:e19673.
http://dx.doi.org/10.7717/peerj.19673
Horn, B.K.P., 1981. Hill Shading and the Reflectance Map. *Proceedings of the IEEE*, 69:14–47.
http://dx.doi.org/10.1109/PROC.1981.11918
IBGE, 2023. *Modelo hgeoHNOR2020 para conversão de altitudes geométricas em altitudes normais*, volume 47 of *Relatórios metodológicos*. Instituto Brasileiro de Geografia e Estatística, Rio de Janeiro, 2. ed. edition. Available only as digital media.
https://biblioteca.ibge.gov.br/index.php/biblioteca-catalogo?view=detalhes&id=2102048
Imhof, E., 1982. *Cartographic relief presentation*. Walter de Gruyter, Berlin.
Infraestrutura de Dados Espaciais do Estado de São Paulo, 2023. Vôo 2023 São Sebastião 10 cm Vila Sahy. São Paulo. Available at https://www.idesp.sp.gov.br/geonetwork/srv/por/catalog.search#/metadata/%7B4A9B4AB9-BBD9-4D6B-8D9D-BFBD679B8042%7D, last access 2025-11-01.
Jasiewicz, J., Stepinski, T.F., 2013. Geomorphons — a pattern recognition approach to classification and mapping of landforms. *Geomorphology*, 182:147 – 156.
http://dx.doi.org/10.1016/j.geomorph.2012.11.005
Koenderink, J.J., van Doorn, A.J., 1992. Surface shape and curvature scales. *Image and Vision Computing*, 10(8):557–564.
http://dx.doi.org/10.1016/0262-8856(92)90076-f
Laipelt, L., Comini de Andrade, B., Collischonn, W., de Amorim Teixeira, A., Paiva, R.C.D.d., Ruhoff, A., 2024. ANADEM: A Digital Terrain Model for South America. *Remote Sensing*, 16(13).
http://dx.doi.org/10.3390/rs16132321
Lindsay, J., 2016. Whitebox GAT: A case study in geomorphometric analysis. *Computers & Geosciences*, 95:75–84.
http://dx.doi.org/10.1016/j.cageo.2016.07.003
Lindsay, J.B., 2018. A new method for the removal of off-terrain objects from LiDAR-derived raster surface models.
https://www.researchgate.net/publication/323003064_A_new_method_for_the_removal_of_off-terrain_objects_from_LiDAR-derived_raster_surface_models
Lindsay, J.B., Dhun, K., 2015. Modelling surface drainage patterns in altered landscapes using lidar. *International Journal of Geographical Information Science*, 29(3):397–411.
http://dx.doi.org/10.1080/13658816.2014.975715
Lindsay, J.B., Francioni, A., Cockburn, J.M.H., 2019a. LiDAR DEM Smoothing and the Preservation of Drainage Features. *Remote Sensing*, 11(16).
http://dx.doi.org/10.3390/rs11161926
Lindsay, J.B., Newman, D.R., Francioni, A., 2019b. Scale-Optimized Surface Roughness for Topographic Analysis. *Geosciences*, 9(7):322.
http://dx.doi.org/10.3390/geosciences9070322
Marengo, J.A., Cunha, A.P., Seluchi, M.E., Camarinha, P.I., Dolif, G., Sperling, V.B., Alcântara, E.H., Ramos, A.M., Andrade, M.M., Stabile, R.A., Mantovani, J., Park, E., Alvala, R.C., Moraes, O.L., Nobre, C.A., *et al.*, 2024. Heavy rains and hydrogeological disasters on February 18th–19th, 2023, in the city of São Sebastião, São Paulo, Brazil: from meteorological causes to early warnings. *Natural Hazards*, 120(8):7997–8024.
http://dx.doi.org/10.1007/s11069-024-06558-5
Mark, D.M., Smith, B., 2004. A science of topography: From qualitative ontology to digital representations. In M.P. Bishop, J.F. Shroder, editors, *Geographical Information Science and Mountain Geomorphology*, July, pages 75–100. Springer, Praxis Publishing, Chichester, England.
Nelson, A., Reuter, H.I., Gessler, P., 2009. Chapter 3 DEM Production Methods and Sources. In T. Hengl, H.I. Reuter, editors, *Geomorphometry: Concepts, Software, Applications*, volume 33 of *Developments in Soil Science*, pages 65–85. Elsevier, Amsterdam.
http://dx.doi.org/10.1016/S0166-2481(08)00003-2
O'Callaghan, J.F., Mark, D.M., 1984. The Extraction of Drainage Networks from Digital Elevation Data. *Computer Vision, Graphics, and Image Processing*, 28:323–344.
http://dx.doi.org/10.1016/S0734-189X(84)80011-0
Organisation for Economic Co-Operation and Development, 2015. Making open science a reality.
http://dx.doi.org/10.1787/5jrs2f963zs1-en
Pike, R.J., Evans, I.S., Hengl, T., 2009. Chapter 1. Geomorphometry: a brief guide. In T. Hengl, H.I. Reuter, editors, *Geomorphometry: Concepts, Software, Applications*, volume 33 of *Developments in Soil Science*, pages 3–30. Elsevier, Amsterdam.
http://dx.doi.org/10.1016/S0166-2481(08)00001-9
Pronk, M., Hooijer, A., Eilander, D., Haag, A., de Jong, T., Vousdoukas, M., Vernimmen, R., Ledoux, H., Eleveld, M., 2024. Deltadtm: A global coastal digital terrain model. In *Scientific Data*, page 111. Springer Nature.
http://dx.doi.org/10.1038/s41597-024-03091-9
Qin, C., Zhu, A., Pei, T., Li, B., Zhou, C., Yang, L., 2007. An adaptive approach to selecting a flow-partition exponent for a multiple-flow-direction algorithm. *International Journal of Geographical Information Science*, 21(4):443–458.
http://dx.doi.org/10.1080/13658810601073240

Sato, E., Vlach, S., Basei, M., 2008. Zircon and baddeleyite upb dating (tims) of mesozoic alkaline rocks from the são sebastião island, southeastern brazil. *International Geological Congress, Oslo*.
https://repositorio.usp.br/item/001717959

Sato, E.N., 2006. *Petrografia e geocronologia U/Pb (TIMS) de rochas alcalinas da Ilha de São Sebastião (SP)*. Ph.D. thesis, Universidade de São Paulo.
https://bdta.abcd.usp.br/item/001662223

Strobl, P., 2020. The new Copernicus digital elevation model. *GSICS Quarterly*, 14(1).
http://dx.doi.org/10.25923/enp8-6w06

Strobl, P.A., Bielski, C., Guth, P.L., Grohmann, C.H., Muller, J.P., López-Vázquez, C., Gesch, D.B., Amatulli, G., Riazanoff, S., Carabajal, C., 2021. The Digital Elevation Model Intercomparison eXperiment DEMIX, a community based approach at global DEM benchmarking. *The International Archives of the Photogrammetry, Remote Sensing and Spatial Information Sciences*, XLIII-B4-2021:395–400.
http://dx.doi.org/10.5194/isprs-archives-XLIII-B4-2021-395-2021

Tachikawa, T., Hato, M., Kaku, M., Iwasaki, A., 2011. Characteristics of ASTER GDEM version 2. In *Geoscience and Remote Sensing Symposium (IGARSS), 2011 IEEE International*,
http://dx.doi.org/10.1109/IGARSS.2011.6050017 pages 3657–3660.

Tadono, T., Takaku, J., Tsutsui, K., Oda, F., Nagai, H., 2015. Status of ALOS World 3D (AW3D) global DSM generation. In *2015 IEEE International Geoscience and Remote Sensing Symposium (IGARSS)*,
http://dx.doi.org/10.1109/IGARSS.2015.7326657 pages 3822–3825.

Tedersoo, L., Küngas, R., Oras, E., Köster, K., Eenmaa, H., Leijen, A., Pedaste, M., Raju, M., Astapova, A., Lukner, H., Kogermann, K., Sepp, T., 2021. Data sharing practices and data availability upon request differ across scientific disciplines. *Scientific Data*, 8(1).
http://dx.doi.org/10.1038/s41597-021-00981-0

Uhe, P., Lucas, C., Hawker, L., Brine, M., Wilkinson, H., Cooper, A., Saoulis, A.A., Savage, J., Sampson, C., 2025. Fathomdem: an improved global terrain map using a hybrid vision transformer model. *Environmental Research Letters*, 20(3):034002.
http://dx.doi.org/10.1088/1748-9326/ada972

Valeriano, M.M., Kuplich, T.M., Storino, M., Amaral, B.D., Mendes, J.N., Lima, D.J., 2006. Modeling small watersheds in Brazilian Amazonia with shuttle radar topographic mission-90m data. *Computers & Geosciences*, 32:1169–1181.
http://dx.doi.org/10.1016/j.cageo.2005.10.019

Varnier, M., 2024. A cloud-based and open-source approach to generate landslide susceptibility maps. *Revista Brasileira de Geomorfologia*, 25(2).
http://dx.doi.org/10.20502/rbgeomorfologia.v25i2.2491

Winsen, M., Hamilton, G., 2023. A Comparison of UAV-Derived Dense Point Clouds Using LiDAR and NIR Photogrammetry in an Australian Eucalypt Forest. *Remote Sensing*, 15(6).
http://dx.doi.org/10.3390/rs15061694